

1 **Extracting the phylogenetic dimension of coevolution reveals hidden**

2 **functional signal**

3

4 Alexandre Colavin^{1,*}, Esha Atolia^{2,*}, Anne-Florence Bitbol^{3,4}, Kerwyn Casey Huang^{5,6,7,+}

5

6 ¹Biophysics Program, Stanford University School of Medicine, Stanford, CA 94305, USA

7 ²Department of Chemical and Systems Biology, Stanford University School of Medicine,

8 Stanford, CA 94305, USA

9 ³Sorbonne Université, CNRS, Institut de Biologie Paris-Seine, Laboratoire Jean Perrin

10 (UMR 8237), F-75005, Paris, France

11 ⁴Institute of Bioengineering, School of Life Sciences, Ecole Polytechnique Fédérale de

12 Lausanne (EPFL), CH-1015 Lausanne, Switzerland

13 ⁵Department of Bioengineering, Stanford University, Stanford, CA 94305, USA

14 ⁶Department of Microbiology and Immunology, Stanford University School of Medicine,

15 Stanford, CA 94305, USA

16 ⁷Chan Zuckerberg Biohub, San Francisco, CA 94158

17

18 *: Co-first authors.

19 *Keywords:* MirrorTree, protein sectors, normalized joint entropy, Direct Information,

20 Average Product Correction, entropy, MreB, H-Ras, ArgS, G6PD, Enolase, MAPK1,

21 Nested Coevolution

22

23 †To whom correspondence should be addressed: kchuang@stanford.edu

24 **Abstract**

25

26 Despite the structural and functional information contained in the statistical coupling
27 between pairs of residues in a protein, coevolution associated with function is often
28 obscured by artifactual signals such as genetic drift, which shapes a protein's
29 phylogenetic history and gives rise to concurrent variation between protein sequences
30 that is not driven by selection for function. Here, we introduce a method for explicitly
31 defining a phylogenetic dimension of coevolution signal, and demonstrate that
32 coevolution can occur on multiple phylogenetic timescales within a single protein. Our
33 method, Nested Coevolution (NC), can be applied as an extension to any coevolution
34 metric. We use NC to demonstrate that poorly conserved residues can nonetheless have
35 important roles in protein function. Moreover, NC improved structural-contact
36 prediction over gold-standard coevolution-based methods, particularly in subsampled
37 alignments with fewer sequences. NC also lowered the noise in detecting functional
38 sectors of collectively coevolving residues. Sectors of coevolving residues identified after
39 NC correction were more spatially compact and phylogenetically distinct from the rest
40 of the protein, and strongly enriched for mutations that disrupt protein activity. Our
41 conceptualization of the phylogenetic separation of coevolution represents an advance
42 from previous pragmatic attempts to reduce phylogenetic artifacts in measurements of
43 coevolution. Application of NC broadens the application of protein coevolution

44 measurements, particularly to eukaryotic proteins with fewer naturally available
45 sequences, and further elucidates relationships among protein evolution and genetic
46 diseases.

47 **Introduction**

48 It has long been appreciated that comparisons among homologous sequences of a protein
49 of interest can provide key information about its function and structure. Just as
50 evolutionarily conserved individual residues are generally crucial to a protein's proper
51 function, the statistical covariation (arising from correlated evolution, i.e. coevolution)
52 between pairs of residues (1, 2) carries information that is useful for predicting structural
53 contacts (3-7) and protein-protein interactions (8-11) and their interfaces (12), intuiting
54 novel protein conformations (5), understanding protein allostery (13), interpreting
55 variants (14), identifying functional domains (15-18), and reprogramming protein
56 specificity (19). However, despite the increasing prevalence of sequencing data, sampling
57 of the phylogenetic tree is necessarily limited and biased. Evolutionary events such as
58 speciation can drive simultaneous changes that are statistically linked but may not reflect
59 relevant functional coupling, for example when they arise from genetic drift. Hence,
60 spurious covariation is more likely to arise in comparisons between distantly related
61 sequences, hindering the ability of such studies to deliver functional insights.

62

63 Of the numerous existing methods for measuring protein coevolution, many implement
64 methods for reducing the effects of phylogenetic noise. Although mutual information is
65 extremely sensitive to the phylogenetic distribution of sequences and the conservation
66 (measured via entropy) of individual positions, normalization by the joint entropy

67 reduces the influence of phylogeny and entropy and improves structural-contact
68 prediction (20). Statistical coupling analysis, which normalizes the covariance matrix by
69 a function of the entropy, provides sufficient information to specify a protein fold (21)
70 and to detect functional domains (6, 18). Direct coupling analysis (DCA) usually involves
71 down-weighting the coevolutionary signal contributions from over-represented
72 sequences, and attempts to deconvolve higher-order correlations to identify directly
73 interacting residue pairs (4, 22). Motivated by the observed strong relationship between
74 a position's average mutual information and the mutual information it exhibits with
75 specific positions, modifications such as the average product correction (APC) subtract
76 this average signal; this correction can be applied to any existing coevolution metric other
77 than mutual information. However, none of these strategies attempt to resolve the
78 evolutionary timescale of coevolution.

79
80 Even with affordable sequencing and widespread environmental sampling, coevolution
81 methods are often limited by the number of naturally occurring protein sequences
82 available. Successful predictions of structural contacts often require several thousand
83 sequences to align (3, 23), which is generally prohibitive for many mammalian proteins.
84 For other proteins, the phylogenetic distribution of available sequences is skewed by
85 sampling and is well recognized as a source of spurious signal in coevolution (20, 24).
86 Thus, methods that enable the separation of functional coupling from phylogenetic and

87 sampling noise would greatly expand the utility of coevolution, particularly for
88 applications to diseases involving human proteins with limited numbers of available
89 sequences.

90

91 Here, we introduce the concept of Nested Coevolution (NC), a correction that leverages
92 a well-defined null hypothesis to accurately measure the coevolutionary signal above
93 what is expected from phylogenetic distribution alone. We determined that NC results in
94 higher fidelity of the coevolutionary signal across gold-standard coevolution-based
95 metrics for structural prediction for many proteins, especially with fewer sequences. In
96 addition, we found that NC improves the detection of spatially contiguous groups of
97 collectively coevolving residues (“sectors”) that are phylogenetically distinct from each
98 other and the protein itself, beyond differences in entropy alone. Finally, sectors
99 identified using NC were enriched for positions at which mutations are maximally
100 deleterious, highlighting the functional significance of signal from our method. Since our
101 method is agnostic to the underlying method of measuring coevolution, we anticipate
102 wide utility for the ability to resolve the temporal dimension of protein coevolution.

103 Results

104

105 *Background model of coevolution reveals temporal dimension of coevolution*

106 To interrogate the contribution of phylogenetic sampling to protein coevolution
107 measurements, we sought to separate the coevolution signal due to inter-clade and intra-
108 clade sequence comparisons (Fig. 1A,B). Given a multiple sequence alignment (MSA) for
109 a protein of interest (Fig. 1Ai), we first measure the total covariation (C_T) between every
110 pair of positions (Fig. 1Aii) using an established metric of residue-residue coupling such
111 as the normalized mutual information (NMI; Fig. 1A) (20):

$$112 \quad C_T^{ij} = (H_i + H_j - H_{ij})/H_{ij}, \quad (1)$$

113 where H_i is the Shannon entropy (a measure of conservation) of position i , and H_{ij} is the
114 joint Shannon entropy of positions i and j . The quantity $H_i + H_j - H_{ij}$ is the mutual
115 information between positions i and j , which measures the coupling between residues
116 (Fig. S1). The NMI residue pair covariation in Eq. 1 is a natural metric choice because
117 normalizing by H_{ij} makes the mutual information independent of conservation (20). Note
118 that our algorithm can be applied to any covariation metric, and as we will show, our
119 main results are robust to metric choice.

120

121 The most straightforward null hypothesis for protein coevolution is that coevolutionary
122 coupling between pairs of proteins is completely absent—that is, that the probability of a

123 position having any particular amino acid identity is independent of any other position's
124 identity. Although this null hypothesis can be evaluated analytically for some methods
125 (SI), other methods have no known closed-form solution for the expected value of the
126 coevolution matrix under these conditions. Hence, we computationally compute the
127 average coevolution signal from many globally resampled MSAs in which each position
128 in each protein in the original MSA is replaced by the equivalent position from another
129 randomly chosen protein (resampled with replacement; Fig. 1Av,vi). We expect any
130 measured coevolution from these resampled matrices to represent signal due simply to
131 the distribution of amino acid identities at each position; any significant difference
132 between the coevolution signal measured in the original MSA and this null hypothesis
133 can potentially be attributed to coevolution.

134
135 However, this initial null hypothesis does not test for the phylogenetic structure of
136 sequences; in the globally resampled MSAs, every sequence is effectively evolutionarily
137 equidistant from one another. Previous attempts to remove the influence of phylogeny
138 such as APC (Fig. 1Aiii), which corrects the covariation matrix by subtracting the product
139 of its mean value across columns and rows for each pair of positions (Fig. 1Aiv), have
140 substantially improved contact prediction (20). However, the APC is a postulated
141 correction that does not directly take into account the phylogenetic structure of an MSA.
142 We sought to construct a null hypothesis-driven background model of the expected

143 coevolution in an MSA in which intra-clade coevolution is explicitly removed. We
144 achieve this goal by generating MSAs by resampling each position from sequences that
145 are closely related (Fig. 1Av,vi), thus removing correlations arising from recent
146 evolutionary history within each clade. We define a clade as the subset of sequences S
147 with a Jukes-Cantor distance below d , which we refer to as the phylogenetic cutoff. For
148 each value of d , we calculate the inter-clade covariation ($C_{S>d}^{i,j}$) from a resampled MSA
149 either analytically or via bootstrapping (Fig. 1Avii, S2A, Methods), where C denotes the
150 chosen covariation measure (e.g. NMI). This inter-clade covariation thus measures the
151 expected value of covariation due solely to the comparison of sequences between clades
152 (Fig. 1B). We then average over many such null hypotheses (over many within-clade
153 resampled MSAs at fixed d), yielding the mean inter-clade covariation matrix ($C_{S>d}$) (Fig.
154 1Aviii), which represents the expected coevolution due to both the distribution of amino
155 acid identities at each position and the phylogenetic structure of the protein MSA (Fig.
156 1B). Significant differences between this background model and the baseline signal
157 measured from the original MSA represent signal that was contained in the intra-clade
158 comparison of closely related sequences. Since the difference between the background
159 model and the baseline signal qualitatively captures the significance of the baseline
160 measurement (Fig S2B, Methods), we subtract $C_{S>d}$ from the total covariation C_T to obtain
161 the phylogenetic cutoff-dependent covariation signal $C_{S\leq d}$ (Fig. 1Aix); positive values
162 indicate that the total covariation is larger than expected by comparison of sequences

163 between clades, thus revealing covariation arising from recent evolutionary history in all
164 clades:

$$165 \quad C_{S \leq d}^{i,j} \equiv C_T^{i,j} - C_{S > d}^{i,j}. \quad (2)$$

166 We refer to the signal $C_{S \leq d}^{i,j}$ above the null hypothesis $C_{S > d}^{i,j}$ in Eq. 2 as a protein's "nested
167 coevolution" (NC), in that it separates coevolution signal into signal attributed to
168 comparison of sequences either within ($C_{S \leq d}^{i,j}$) or between ($C_{S > d}^{i,j}$) nested clades of a
169 phylogenetic tree. The only free parameter in the NC is the phylogenetic cutoff (d). As
170 we vary the cutoff value, many patterns of NC typically emerge, revealing distinct
171 windows of coevolution for a single protein MSA (Fig. 1C). The changes in NC observed
172 between two cutoffs represent the signal due to pairs of sequences whose distance is
173 between the cutoffs used to calculate each window. Hence, distinct evolutionary
174 timescales of protein coevolution are revealed as the phylogenetic cutoff is varied.

175
176 To test the relevance of NC windows to protein structure prediction, we measured the
177 enrichment of structural contacts from the pairs of residues with the highest 50 values in
178 the NC matrix $C_{S \leq d}^{i,j}$ for each value of d . Here, we applied NC as a correction to DCA, the
179 current gold standard for coevolution-based prediction of structural contacts (4, 22). We
180 employed the direct information (DI) metric to quantify coevolution (4, 22). In this and
181 subsequent analyses, we considered structural contacts to be within 5 Å at closest
182 approach, excluding pairs of residues within 5 amino acids on the sequence (Methods).

183 The NC phylogenetic cutoffs revealed a variety of improvements for the KH domain (Fig.
184 1D), which is present in a wide variety of nucleic acid-binding proteins (25). Some
185 windows generally outperformed DCA, without (Fig. 1E) or with (Fig. 1F) the APC.

186
187 To determine the added value of NC for other proteins and for another frequently utilized
188 coevolution metric, the Frobenius norm (26), which is frequently utilized in DCA as an
189 alternative to DI (27, 28), we carried out a DCA structural-contact analysis for 10 protein
190 family domains with DI or Frobenius norm (Methods). Across both metrics and all
191 proteins, NC improved the predictions of structural contacts (Fig. 2A), even relative to
192 the inclusion of APC (20). Hence, NC is a correction that enhances the predictive power
193 of state-of-the-art coevolution measurements.

194

195 *NC improves predictions of structural contacts using fewer sequences*

196 One common limitation for computing coevolution is the number of homologous
197 sequences available for constructing an MSA. To interrogate whether NC could still
198 accurately predict structural contacts with fewer sequences, we subsampled the MSAs of
199 10 proteins with different breadth (randomly selecting 10% or 1% of the sequences) or
200 depth (selecting the 10% or 1% of sequences most related to the protein used to construct
201 the MSA, Table S1) (Fig. 2B). NC improved structural contact prediction for a majority of
202 the subsampled MSAs when correcting DI without (Fig. 2C, S4A) or with (Fig. S3B)

203 application of APC. For the KH domain, more than twice as many true positives were
204 predicted after applying NC compared with DI+APC alone (Fig. S3A). Perhaps
205 unsurprisingly, breadth sampling generally performed better than depth sampling (Fig.
206 2C), indicating that accurate prediction is reliant on the sequences being sufficiently
207 distantly related. Nonetheless, for many proteins, the value of the NC correction was
208 enhanced when the number of homologous sequences was low, both for depth and
209 breadth samplings.

210

211 *NC generates eigenvectors with increased fidelity, improving detection of spatially*
212 *contiguous sets of coevolving residues*

213 Previous studies have utilized coevolution measurements to identify groups of residues
214 within a protein that are spatially contiguous on the tertiary structure and thus are
215 postulated to have a joint function (6, 18, 29-32). These “sectors” can be defined by a
216 variety of methods, such as the extreme-value residues of the eigenvectors of the
217 coevolution matrix with the largest eigenvalues (18), and have been proposed to reflect
218 independent biological properties such as catalytic efficiency and thermal stability (18).
219 Motivated by these successes, we sought to measure the effect of incorporating the
220 phylogenetic dimension revealed by NC when defining sectors of residues. Specifically,
221 we measured the NC- and APC-corrected coevolution using NMI across a range of
222 phylogenetic cutoffs, concatenating the results and performing eigendecomposition to

223 identify the most significant eigenvectors (Methods). The residues most strongly
224 associated with the positive or negative components of each resulting eigenvector are
225 considered a sector.

226

227 We first focused on MreB, an essential protein involved in cell-shape determination in
228 many rod-shaped bacteria (33). MreB belongs to a protein family that includes ParM,
229 FtsA, and MamK in bacteria, crenactin in archaea, and actin in eukaryotes (34, 35). These
230 proteins are structural homologs characterized by a four-subdomain fold around an ATP-
231 binding pocket (35, 36), with very low sequence identity and disparate cellular functions.
232 Thus, we anticipated that the set of MreB homologs would have sufficient diversity to
233 support robust coevolution measurements, particularly functional sectors.

234

235 We compared NC-derived sectors with baseline sectors derived from eigenvectors of the
236 baseline coevolution matrix for MreB homologs. We identified the most closely related
237 baseline sectors for three NC eigenvectors with some of the highest eigenvalues, which
238 we refer to as eigenvectors A, B, and C (Methods). Each pair of NC and baseline
239 eigenvectors appeared similar, especially for the residues with the largest absolute
240 coefficients (Fig. 3A-C). However, the baseline eigenvectors exhibited much higher
241 variation of coefficients for residues across the protein (Fig. 3A-C). For eigenvectors A
242 and B, the NC-derived eigenvectors exhibited 32.8-fold and 38.3-fold lower standard

243 deviation (after removing the 50 highest and lowest coefficients) than the baseline-
244 derived eigenvectors, respectively (Fig. 3A,B). For eigenvector C, the baseline eigenvector
245 contained residues with both highly positive and highly negative coefficients, while the
246 high-magnitude coefficients of the NC eigenvector were solely positive (Fig. 3C); the
247 positive portion of the NC eigenvector again had substantially lower noise than the
248 baseline eigenvector (2.1-fold lower standard deviation, Fig. 3C).

249
250 Motivated by the distinct behaviors of the positive and negative components of
251 eigenvector C, we defined distinct positive and negative sectors (Methods) for each NC
252 and baseline eigenvector using a variable cutoff on the site contributions to adjust sector
253 size (as sectors are defined as the sets of amino acids with highest site contributions in a
254 given eigenvector). For different sector sizes, we quantified the spatial contiguity as the
255 mean pairwise distance between each residue within a sector. For sectors A-C (derived
256 from eigenvectors A-C), the first 5-9 residues exhibited approximately the same spatial
257 contiguity in the NC as in the baseline eigenvectors (Fig. 3D-F). However, as the cutoff
258 was increased, the NC sector remained more spatially compact than the baseline sector
259 (Fig. 3D-F). All three NC sectors were also more spatially contiguous than expected based
260 on random sampling for cutoffs yielding at least 50 residues (Fig. 3D-F), while the
261 baseline sector A was distributed across the protein structure (Fig. 3D,J). NC sectors A
262 and C were largely situated in subdomains IIA (Fig. 3G) and IA (Fig. 3I), respectively,

263 while sector B was localized to the ATP-binding pocket (Fig. 3H). Notably, sector C was
264 spatially contiguous (Fig. 3I) despite being spread across the protein sequence (Fig. 3C).
265 Baseline sectors B and C with 15 residues were qualitatively similar to the corresponding
266 NC sectors (Fig. 3K,L); the large background fluctuations of the baseline eigenvector
267 likely led to the inclusion of additional, erroneous residues into the sector prediction.
268 Thus, the phylogenetic correction of NC improves the fidelity of sector detection as
269 measured by the spatial contiguity of its constituent residues.

270

271 *Sectors display distinct phylogenetic signatures from the rest of the protein*

272 Since sectors have been postulated to reflect distinct evolutionary histories driven by
273 selection for particular biological functions (18), we sought to compare the phylogeny of
274 the residues within a sector with other sectors and the rest of the protein. The MirrorTree
275 algorithm (Methods) was originally developed to compare phylogenies of two proteins,
276 motivated by the assumption that similar histories signifies a common function, e.g.
277 through protein-protein interactions and/or acting in the same pathway (37, 38). After
278 computing a pairwise distance matrix of all sequences within an MSA for each of the two
279 proteins based on homologs in the same set of organisms, the MirrorTree score is defined
280 as the Pearson correlation coefficient between the entries in the two pairwise distance
281 matrices (37). We straightforwardly modified the MirrorTree method to compare the

282 complete protein MSA to the MSA filtered to include only the residues within the sector
283 of interest (Fig. 4A).

284

285 To broadly investigate sector identification, we identified 40 15-residue sectors for MreB
286 based on the positive and negative coefficients of the 20 eigenvectors with the highest
287 eigenvalues. As negative controls, we randomly sampled sets of residues of the same size
288 as each sector from across the protein. Sector-protein MirrorTree scores for sectors A-C
289 (Fig. 3) were substantially lower for sectors than for the random groups (Fig. 4B), which
290 all had MirrorTree scores close to 1, as expected (Fig. 4B). Baseline sectors A-C had
291 MirrorTree scores intermediate between those of the corresponding NC sector and
292 random groups (Fig. 4B), likely reflecting the noisy selection from baseline eigenvectors
293 of residues that functionally follow the phylogenetic history of the protein overall. To
294 evaluate the significance of the MirrorTree score and of the spatial contiguity of each
295 sector, we computed z-scores based on the mean and standard deviation of the two
296 metrics applied to the random groups of the same size as each sector. Sectors A-C had
297 MirrorTree scores <0.5 (Fig. 4B), indicating distinct phylogenetic histories from the
298 protein, and MirrorTree and spatial contiguity z-scores <-2 (Fig. 4C). There were four
299 other sectors (D-G) that had spatial contiguity z-scores <-2 . These sectors largely
300 overlapped with A-C; we will return to this overlap in a later section. All other sectors
301 had spatial contiguity z-score >2 , and all but five (H-L) had MirrorTree z-score >-2 . Thus,

302 MirrorTree reveals that certain NC sectors have distinct evolutionary trajectories from
303 the protein itself, motivating us to focus on certain sectors (such as A, B, and C for MreB).

304

305 *Phylogenetic similarity and the role of entropy*

306 Conservation itself is a major determinant of protein function (39-41), and spatially
307 contiguous sets of residues can be identified solely on the basis of conservation (42). To
308 account for variation in entropy across a protein, previous studies have excluded
309 positions with high conservation (Shannon entropy <0.1) or composed of $>25\%$ gaps in
310 the MSA (43). For MreB, NC sectors A-C had lower entropy than baseline sectors or
311 random groups of the same size (Fig. 5A-C), albeit higher entropy than residues typically
312 considered highly conserved (entropy <0.1).

313

314 MirrorTree scores of NC sectors were also generally lower than those of baseline sectors
315 (Fig. 5D-F). To investigate the dependence of sector-protein MirrorTree scores on
316 entropy, we computed MirrorTree scores for thousands of random groups of the same
317 size as the sector (15 residues), biasing sampling using a Monte Carlo algorithm to obtain
318 a wide range of mean entropies; each random group was selected from residues that did
319 not overlap with the sector. For mean entropy $\lesssim 1$, MirrorTree scores were strongly
320 dependent on entropy (Fig. 5G-I). Thus, the low MirrorTree scores of the NC sectors were
321 due in part to their low entropy. Nonetheless, the MirrorTree score of NC sector A was

322 significantly lower than those of random groups with the same mean entropy (z-score -
323 3.5); the entropy of sector B was so low, presumably due to the high conservation of the
324 ATP-binding pocket (Fig. 3H, S4), that it was challenging to obtain random groups that
325 were not largely overlapping.

326

327 Since NC sector A displayed the greatest reduction in MirrorTree score relative to
328 random groups of the same mean entropy, we focused on this sector to investigate the
329 dependence of the sector-protein MirrorTree score on sector size. As the cutoff was
330 increased to include more residues, the MirrorTree score increased (Fig. 5D). To
331 disentangle whether this increase was due directly to the increase in size or to the
332 inclusion of residues that are more phylogenetically similar to the protein, we compared
333 the 10-residue version of sector A (Fig. 5G) with randomly selected groups of 10 residues
334 from 15- and 20-residue versions of sector A, as well as the entire protein. The mean
335 MirrorTree score increased as the size of the sampling group increased (Fig. 5J), even for
336 groups with similar entropy as the 10-residue sector (Fig. 5K). Moreover, 15-residue
337 versions of sectors B and C had similar entropy (Fig. 5B,C); hence, an approach driven by
338 entropy alone would not have divided these spatially separated clusters. Thus, the
339 strength of a residue's association in a sector of highly coevolving residues is associated
340 with more phylogenetic distinction from the rest of the protein than can be explained by
341 entropy alone.

342

343 *Phylogenetic similarity highlights overlapping sectors*

344 The core residues of some MreB NC eigenvectors sometimes had high coefficients in
345 multiple eigenvectors (Fig. S5), suggesting that we should consider the union of the
346 sectors as a functional unit. To rationally identify sectors that should be merged, we again
347 exploited phylogenetic similarity by calculating MirrorTree correlation coefficients from
348 comparisons between pairs of sectors (Fig. 6A). MreB NC sectors A-C (Fig. 3) exhibited
349 low sector-sector MirrorTree scores with each other and with random groups (Fig. 6B),
350 as expected since they have low sector-protein MirrorTree scores (Fig. 6B). By contrast,
351 the random groups had MirrorTree scores close to 1 (Fig. 6B). NC sectors were also more
352 phylogenetically distinct from each other than baseline sectors (Fig. 6C). These data
353 suggest that the NC sectors were selected by evolutionary pressures that led to distinct
354 functions.

355

356 Of all sectors that had a MirrorTree z-score or a pairwise distance z-score < -2 (sectors A-
357 L, Fig. 4C), several pairs had a high sector-sector MirrorTree score. Hierarchical clustering
358 of the sectors based on their sector-sector MirrorTree profiles led to the identification of
359 five obvious “mega-sectors” from the sum of the clustered eigenvectors (Methods), which
360 we denote α , β , γ , δ , and ε (α , β , and γ contain sectors A, B, and C, respectively) (Fig. 6D).
361 The mega-sectors exhibited low sector-sector MirrorTree scores (Fig. 6E), and α , β , and γ

362 had both low sector-protein MirrorTree scores (Fig. 6F, G) and low spatial contiguity z-
363 scores (Fig. 6G). The 15-residue version of mega-sector α more compact than the 15-
364 residue version of A (Fig. 6H), and it contained residues that interact with RodZ (Fig. 6I),
365 an MreB binding partner that modulates MreB filament nucleation (44) and curvature
366 (45). Notably, the regions of the 25-residue version of mega-sector α at the barbed and
367 pointed ends of the MreB subunit interact with each other in a polymerized MreB
368 filament (Fig. 6J), reinforcing the spatial contiguity of the mega-sector. Mega-sector β was
369 identical to sector B, surrounding the ATP-binding pocket (Fig. 6K). As with α and A, the
370 15-residue version of mega-sector γ was more compact than the 15-residue version of
371 sector C (Fig. 6L), indicating that clustering based on MirrorTree scores increases the
372 spatial contiguity of sectors.

373

374 *NC identifies sectors that are not apparent from the full coevolution matrix*

375 To determine whether our findings about the properties of NC sectors applied to other
376 proteins, we performed similar sector calculations for enolase (the metalloenzyme
377 responsible for conversion of 2-phosphoglycerate to phosphoenolpyruvate during
378 glycolysis (46); Fig. 7A-C), the carbohydrate-processing enzyme glucose-6-phosphate
379 dehydrogenase (G6PD (47); Fig. 7D-F), and mitogen-activated protein kinase 1 (MAPK1
380 (48, 49) (Fig. 7G-K). In each case, NC produced sectors with lower background noise and
381 higher spatial contiguity than baseline sectors.

382

383 Most of the MreB NC eigenvectors had strong signal for either positive or negative
384 coefficients, but not both (Fig. 3A-C). By contrast, one of the large-eigenvalue NC
385 eigenvectors for MAPK1 had groups of residues with both very positive and very
386 negative coefficients (Fig. 7G); these residues were located in distinct regions of the
387 protein (Fig. 7J,K). As validation for splitting the NC eigenvector into two sectors, the
388 sector-sector MirrorTree score (0.44) indicated that they are phylogenetically distinct;
389 moreover, the sector-sector MirrorTree score of the corresponding baseline sectors was
390 higher (0.71). Thus, NC eigenvectors can be interpreted as two phylogenetically distinct
391 sectors based on coefficient signs.

392

393 In addition to improving sector predictions by reducing background variation, we were
394 interested in determining whether NC is able to identify sectors that the full coevolution
395 matrix misses altogether. For the arginine tRNA ligase ArgS (50) and G6PD, the sector
396 with the most negative MirrorTree z-score had nearly the lowest spatial contiguity z-
397 scores (Fig. 7L,M) and no clear counterpart in any of the baseline eigenvectors (Methods).
398 For ArgS, the NC sector was spatially localized around the arginine binding site (Fig. 7N).
399 For G6PD, the NC sector was adjacent to one of the two NADPs that bind to the protein
400 (Fig. 7O). Thus, the NC correction reveals some sectors that are missed by the baseline
401 method.

402

403 *NC sectors are enriched in damaging mutations*

404 To test the functional significance of NC sectors, we sought experimental datasets with
405 quantitative measurements of the consequences of mutations across a protein of interest.
406 Recent studies have pioneered the use of deep mutational scanning to systematically
407 generate and quantify the phenotypic or fitness effects of a large number of individual
408 mutations spanning entire domains or protein (29, 51-53), providing new insights into
409 structure-function relationships. Thus, we asked whether NC sectors were enriched in
410 residues for which mutation altered protein function and/or fitness.

411

412 The Ras superfamily of membrane-associated small G-proteins is highly conserved and
413 controls a broad range of cellular processes (54), has inactive and active states that are
414 regulated by a GTPase-activated protein (55), and has been implicated in cancer (56). A
415 recent deep mutational scanning study engineered plasmids to express mutant versions
416 of human H-Ras as well as the Ras-binding domain of human C-Raf (Raf-RBD) in
417 *Escherichia coli* (57), such that the binding of Ras-GTP to Raf-RBD led to transcription of a
418 chloramphenicol-resistance cassette. Thus, the binding efficacy of the Ras variant was
419 directly correlated with cellular growth rate. The effect of Ras mutations on fitness was
420 quantified by the logarithm of the enrichment of variants in the chloramphenicol-selected
421 versus the starting population, relative to wild-type. The distribution of fitness effects

422 was centered around zero, although there were some positions with mutations that
423 displayed significant functional effects (57).

424

425 To determine whether fitness-altering mutants in H-Ras are enriched at positions
426 identified by coevolution, we identified two high-eigenvalue sectors with obvious
427 corresponding baseline sectors. As in our previous analyses (Fig. 3A-C, 7A,D,G), aside
428 from the highly coevolving residues, the NC sectors had much lower noise than the
429 baseline sectors (Fig. 8A,B). The residues in the two NC sectors were non-overlapping,
430 and in both cases appeared to be concentrated in regions with low minimum relative
431 enrichment (Fig. 8C,D). Across cutoffs that defined sectors of various sizes, we computed
432 the minimum and maximum relative enrichment (representing deactivation and
433 activation, respectively) over all amino acid mutations for each position in the
434 NC/baseline sectors as well as for the residues with the lowest entropy, and compared to
435 the distribution over all residues. As expected, the residues with lowest entropy
436 consistently predicted significantly more negative minimum relative enrichment than
437 random sets of residues (Fig. 8E,F). The mean minimum relative enrichment in NC and
438 baseline versions of sector A was also significantly more negative than random residues,
439 with the NC sector outperforming the baseline sector and achieving similar enrichment
440 values to the lowest-entropy residues (Fig. 8E). NC sector B also exhibited mean
441 minimum relative enrichment significantly lower than random, by contrast to the

442 baseline sector (Fig. 8F). Thus, sectors A and B are more enriched for residues whose
443 mutation has the most potential for reducing fitness using NC versus baseline. The
444 maximum relative enrichment was highly similar for sectors and the protein overall (Fig.
445 S6A,B), suggesting that NC and baseline sectors are enriched for residues with the
446 potential for deactivating rather than activating mutations in the case of H-Ras. Thus, NC
447 sectors separate residues based on the maximum impact of mutations at these positions.

448 **Discussion**

449

450 Many existing coevolution methods build on correlation or mutual information,
451 sometimes employing ad-hoc corrections to partially remove the effects of entropy and
452 phylogeny. Our NC method harnesses phylogenetic distance between sequences as a
453 novel dimension in the measurement of protein coevolution, in order to increase
454 understanding of the functional relationships between amino acids in a protein. In
455 particular, here we demonstrated that coevolution can occur on multiple phylogenetic
456 timescales within a single protein. While the factors that determine whether pairs of
457 positions coevolve on short or long timescales are unknown, future studies using NC to
458 interrogate the specific biochemical functions of protein sectors may reveal general
459 patterns across diverse proteins. One interpretation of the variable contribution of
460 coevolution across phylogenetic distance within a single protein (Fig. 1C) is that the
461 frequency of mutation for coevolving residues within an NC sector is linked to the
462 timescale of change for the corresponding selective pressure on that sector. For example,
463 a sector that determines protein thermostability would be predicted to coevolve on a
464 timescale commensurate with the frequency of changes in environmental temperature,
465 whether these changes occur over long (e.g. glaciation and interglacial cycles of 100,000
466 years) or shorter (e.g. Atlantic multidecadal oscillations) timescales.

467

468 Importantly, NC and our repurposed MirrorTree methods are complementary to most
469 covariation metrics, and hence can enhance existing bioinformatics tools by defining a
470 phylogenetic dimension of coevolution and allowing focus on functional signal. We
471 anticipate that our approach will enable application of coevolution-based methods across
472 a much broader class of proteins, including those for which the set of sequences is limited
473 in number (Fig. 2) and/or for which the available homologous sequences are biased to a
474 particular segment of the phylogenetic tree (Fig. 1B). In particular, application to the
475 growing database of human exome sequences (58) may improve identification of rare
476 disease-causing mutations. NC may also enhance protein engineering tools by
477 highlighting targets for directed evolution. As we have demonstrated, NC expands our
478 ability to detect functional relationships between residues within proteins and to
479 determine the links between protein evolution and adaptation. In concert with deep
480 mutational scanning and other comprehensive functional screens (59), NC and
481 MirrorTree should provide deeper insight into the specific selective pressures under
482 which proteins have evolved.

483

484 The predominant application of coevolution so far has been structure prediction, from
485 using top DCA-predicted contacts as constraints (4) to employing DCA model
486 parameters as input training features for deep neural networks that seek to predict spatial
487 distances between amino acids (60). Here, we have shown that NC can improve contact

488 prediction by DCA. Moreover, the detection and interpretation of sectors as functional
489 units within proteins has been a growing research focus, particularly with respect to the
490 evolutionary origins of sectors. A recent theoretical study demonstrated that selection
491 acting on a functional property can give rise to a sector (28). Here, we showed that NC
492 better resolves sectors than baseline by reducing background noise (Fig. 3A-C), leading
493 to sectors with higher spatial contiguity (Fig. 3D-L) and lower MirrorTree scores (Fig. 4B).
494 Low MirrorTree scores reveal that residues within sectors have a different evolutionary
495 history from the rest of the protein, due to both entropy-dependent and entropy-
496 independent differences (Fig. 5). MirrorTree scores can further be used to evaluate NC
497 predictions in the absence of a known structure. Motivated by the original design
498 purpose of MirrorTree, we note that scores between sectors of two proteins could be used
499 to identify protein-protein interactions—potentially between hosts and microbes—due to
500 the improved performance of NC when the sampling of sequences is shallow (Fig. 2C).

501
502 Our observation that NC sectors, and moreover their cores, have high spatial contiguity
503 and low MirrorTree scores (Fig. 5J) supports the inferred link between coevolution and
504 spatial contiguity, and suggests that NC can help to guide experiments toward the
505 residues of highest importance for a sector's function (Fig. 8). Beyond the improvements
506 from lowering background signal, NC also predicts sectors that are otherwise difficult to
507 detect (Fig. 7L-O), thus highlighting its value. In addition, some studies have

508 demonstrated other applications such as protein engineering (19) and variant
509 interpretation (14). Improved detection of functional coevolution could even help to
510 refine MSA algorithms, which are ultimately a limiting factor in the detection of
511 coevolution. Our results suggest that the utility of coevolution as a signal for protein
512 science can be substantially improved by NC, opening new windows for broadly
513 understanding (and perhaps ultimately engineering) protein structure-function
514 relationships.

515 **Methods and Materials**

516

517 **MSA construction**

518 MSAs were constructed with BLAST (61) to identify up to 10,000 closest sequences to a
519 reference sequence, using the RefSeq database (62). Sequences were aligned with Clustal
520 Omega (63). Sequences with a Jukes-Cantor distance >1 from the reference sequence were
521 pruned. Redundant sequences and positions with $>25\%$ gaps were removed. Any
522 remaining gaps were filled with the closest amino acid from the closest sequence in terms
523 of Jukes-Cantor distance.

524

525 **Calculation of the expected value of inter-clade covariation**

526 For our analyses, we define a pair of sequences to be within the same clade if the
527 phylogenetic distance is below a Jukes-Cantor distance d . The phylogenetic distance is
528 measured with respect to the aligned protein sequence (Table S1). We sought to measure
529 the expected value of residue-residue covariation due solely to the comparison of
530 sequences between clades, which we refer to as the inter-clade covariation $C_{S>d}$. Below,
531 we describe and compare measurement of the expected value of inter-clade covariation
532 in Eq. 1 of the main text both by approximation via bootstrapping and analytically.

533

534 *Bootstrapping*

535 In this approximate method, we bootstrap the original MSA: for every position, we
536 replace the amino acid with the identity of the same position from a random sequence in
537 the same clade. For example, in Fig. 1Avi we show two positions in an MSA, colored by
538 their clade membership for a given phylogenetic distance d . Note that the first position is
539 never a glutamine in the orange clade and is never a threonine in the white clade.
540 Similarly, the second position is never a serine in the orange clade and is never an
541 arginine in the white clade. The bootstrapped MSAs resample within clades, so as to not
542 change the phylogenetic structure of the MSA at distances $>d$; thus, the first position in
543 the bootstrapped MSAs still does not contain a glutamine, etc. The covariation measured
544 from each of the bootstrapped MSAs is averaged to obtain the matrix expected under the
545 hypothesis that there is no coupling between positions within the same clade. The
546 bootstrapping method can be applied for any coevolution heuristic.

547

548 *Analytical method*

549 To derive an analytical solution in place of bootstrapping the NMI metric, we rephrased
550 our aim as calculating the expected value of covariation between two positions under the
551 assumption that the two positions are independent within a clade.

552

553 Consider the Shannon entropy for position i :

554

$$H_i = - \sum_{k=1}^{20} p_{i=k} \ln p_{i=k},$$

555 where $p_{i=k}$ is the probability of finding amino acid k at position i . The marginal
556 probabilities of positions i and j taking on a particular value in a bootstrapped MSA do
557 not change on average. However, the joint entropy, which relies on the joint probability,
558 will change:

559

$$H_{ij} = - \sum_{k,l=1}^{20} p_{i=k,j=l} \ln p_{i=k,j=l}.$$

560 We seek an expression for the joint entropy that captures the assumption that positions i
561 and j are independent within clades. Since the joint probability of independent variables
562 is the product of the individual probabilities, we are left with calculating the sum of
563 probabilities from each clade c , weighted by the number of sequences n_c in each clade:

564

$$p_{i=k,j=l}^{\text{null}} = \left(\sum_c n_c p_{i=k}^c p_{j=l}^c \right) / \left(\sum_c n_c \right)$$

565 where $p_{i=k}^c$ is the marginal probability of finding amino acid k within clade c at position
566 i .

567

568 A comparison of the bootstrapped and analytical methods for calculating NC for the
569 yeast actin protein is shown in Fig. S2.

570

571 *Estimating the statistical significance of nested coevolution*

572 The expectation value of our nested coevolution background model is described above
573 analytically only for normalized mutual information; other coevolution metrics do not
574 have a known closed form analytical solution, so we rely on bootstrapping to estimate
575 the expected value. Bootstrapping offers the additional advantage of providing an
576 estimate of the statistical significance of the observed raw coevolution signal by
577 measuring what fraction of bootstrapped MSAs achieve equal or greater coevolution
578 values. The accuracy of the significance estimate is limited by the number of bootstrap
579 measurements, since the maximum resolution is the reciprocal of the number of
580 bootstraps performed. Using hundreds of bootstraps, we compared significance
581 estimates with the absolute difference between the total and inter-clade covariation.
582 These values were highly correlated (Spearman's $\rho = 0.95$, Fig. S2B), indicating that either
583 the bootstrapping or analytical method of computing NC provides a surrogate for the
584 significance of the observation.

585

586 **Structural contact prediction**

587 Real structural contacts were determined by calculating the distance between the alpha
588 carbons of every pair of residues in the protein based on a crystal structure (Table S1).
589 All other atoms, including hydrogen atoms, were disregarded. To predict structural
590 contacts, we used mean-field DCA, and the value of the pseudocount is 0.5, and
591 sequences closer than 0.3 Hamming distance are reweighted (4, 22).

592

593 **Generation of NC sectors**

594 The output of NC is n_d p -by- p matrices (Fig. 1C), where n_d is the number of phylogenetic
595 windows and p is the number of amino acids in the protein. These n_d matrices are
596 concatenated to obtain a supermatrix of dimension pn_d -by- p (Fig. S7). Principal
597 component analysis using eigenvalue decomposition or singular value decomposition is
598 performed on the super matrix (thus avoiding the need to choose one value of the cutoff
599 distance d), with pn_d observations and p features. The eigenvectors are ordered highest to
600 lowest according to their associated eigenvalues. Each eigenvector is of length p , where
601 the i^{th} coefficient corresponds to the importance of the i^{th} amino acid in explaining the
602 variation in the direction of the respective eigenvector.

603

604 To extract the specific amino acids that are most responsible for explaining the variation
605 in a particular eigenvector, we identify the positions with the most positive or most
606 negative coefficients and define these groups of residues as two sectors. Sectors that have
607 <4 amino acids are ignored for downstream analysis.

608

609 NC and baseline sectors were paired if the dot product of the corresponding eigenvector
610 was >0.6 .

611

612 **Calculating the spatial contiguity of a sector**

613 To quantify spatial contiguity, we calculate the mean distance between the alpha carbon
614 atoms of each pair of residues in the sector in the crystal structure.

615

616 **Adaptation of the MirrorTree algorithm**

617 Mirrortree was originally developed to predict protein-protein interactions based on the
618 similarity of phylogenetic trees (37). In brief, MSAs are calculated using protein
619 sequences from the same list of organisms for two proteins. For each MSA, the matrix of
620 pairwise Jukes-Cantor distances is calculated. The MirrorTree score is the Pearson
621 correlation coefficient of these two distance matrices. A high correlation indicates that the
622 two proteins have similar phylogenies and thus are likely to have experienced similar
623 functional selection. We adapted this method to compare the phylogenetic similarity of
624 protein sectors with the entire protein (Fig. 4A) or other sectors (Fig. 6A). To compute
625 sector-protein and sector-sector MirrorTree scores, filtered MSAs were created focusing
626 on the positions of a given sector.

627

628 Biased sampling of random sectors was accomplished via weighting of residues
629 according to their entropy.

630

631 **Calculation of megasectors**

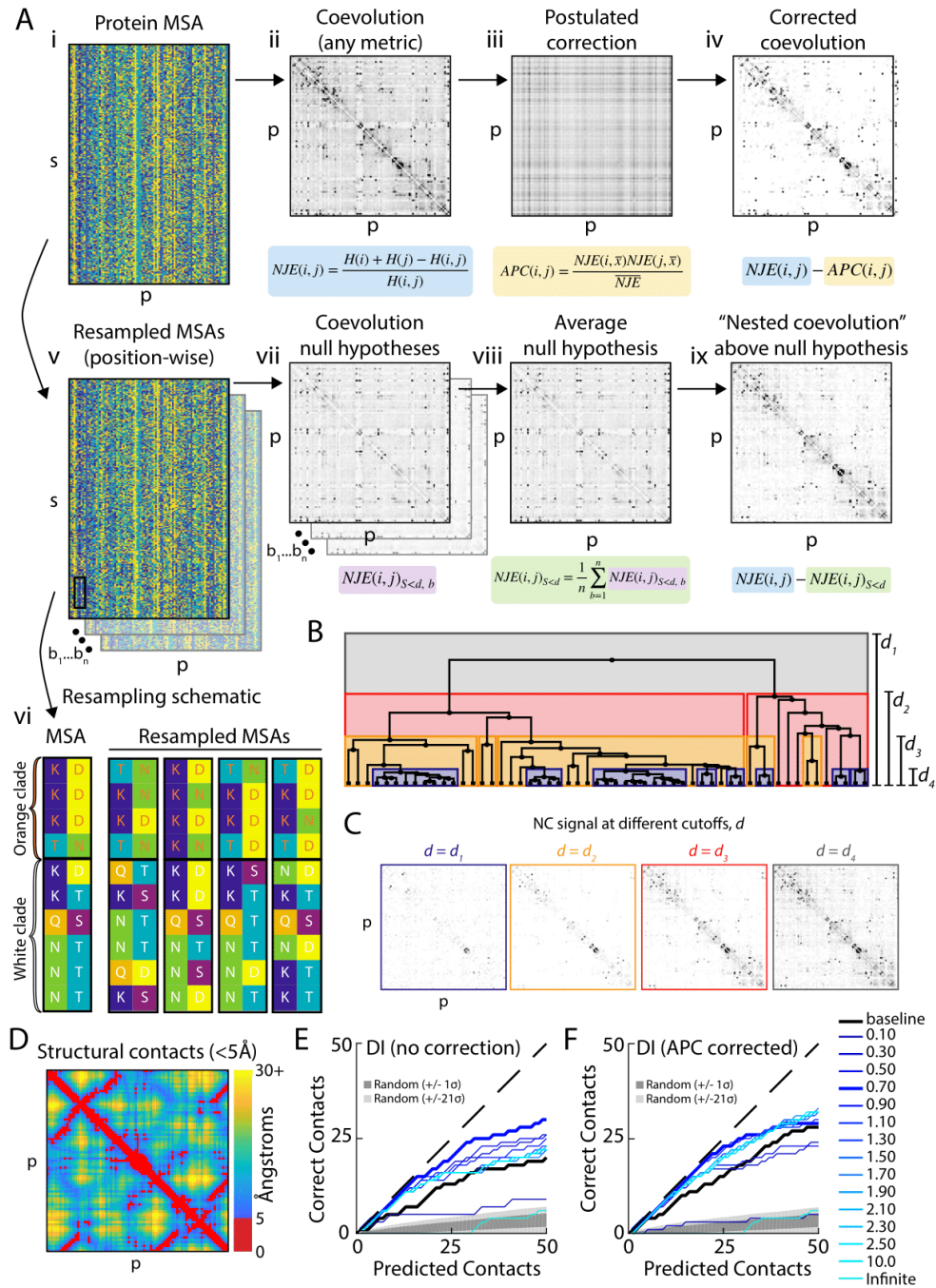
632 Sets of sectors to be merged into megasectors were determined from hierarchical
633 clustering based on sector-sector MirrorTree scores. Merging was accomplished by
634 adding the corresponding eigenvectors after multiplying each sector by +1 or -1
635 corresponding to whether a positive or negative sector, respectively, was being merged.
636 The summed vector was then analyzed as if it were an eigenvector in order to define
637 megasectors at various size cutoffs.

638 **Acknowledgments**

639 The authors thank the Huang lab for useful discussions. This work was supported by
640 Stanford Graduate Fellowships (to A.C. and E.A.), a Gerald J. Lieberman Fellowship (to
641 A.C.), grant 851173 from the European Research Council under the European Union's
642 Horizon 2020 research and innovation programme (to A.-F.B.), NSF CAREER Award
643 MCB-1149328 (to K.C.H.), and the Allen Discovery Center at Stanford on Systems
644 Modeling of Infection (to K.C.H.). K.C.H. is a Chan Zuckerberg Biohub Investigator.

645 **Figure Legends**

646



647

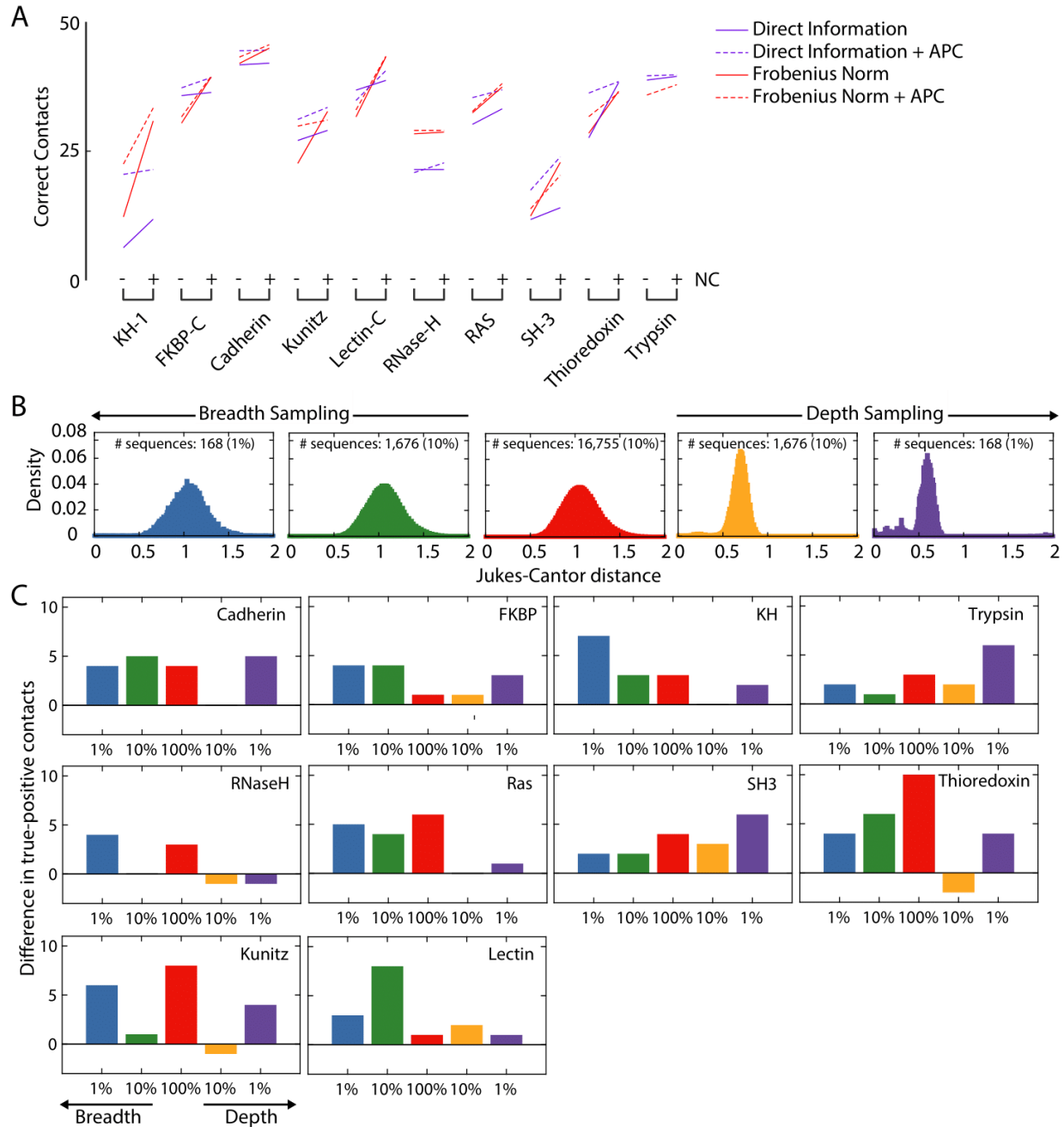
648 **Figure 1: NC introduces a phylogenetic dimension to traditional coevolution metrics**

649 **that removes noise and improves structural prediction.**

- 650 A) Schematic illustrating the NC correction to traditional coevolution algorithms. The
651 MSA (i) is used to generate a covariation matrix (ii) with a particular metric such
652 as normalized joint entropy or direct information. Previous studies have
653 attempted to remove phylogenetic noise using the APC (iii), which results in a
654 corrected coevolution matrix (iv) that has lower levels of off-diagonal signal. For
655 the NC correction, the MSA is resampled multiple times (v) within clades defined
656 by a phylogenetic cutoff d (vi), providing null hypotheses (vii) that are averaged
657 (viii) to correct the covariation matrix (i). The resulting difference (ix) is the NC
658 matrix for a particular cutoff d .
- 659 B) The Jukes-Cantor phylogenetic distance between homologs defines clades
660 (visualized as a tree) within the NC cutoff d .
- 661 C) NC signal at different cutoffs d as illustrated in (B) for the MSA of the KH domain
662 from (B). For small values of d , the NC matrix exhibits very little off-diagonal
663 signal, signifying a reduction in noise.
- 664 D) The structural contact map for KH, highlighting contacts that are in close 3D
665 proximity ($<5 \text{ \AA}$, red), respectively.
- 666 E,F) NC with particular cutoffs d improves the prediction of structural contacts
667 relative to DCA, applied to DI without (E) or after correction with APC (F) (black
668 lines). All residues within five positions on the polypeptide sequence were

669 excluded from the analysis. Gray represents the predictions of the baseline NMI

670 metric.



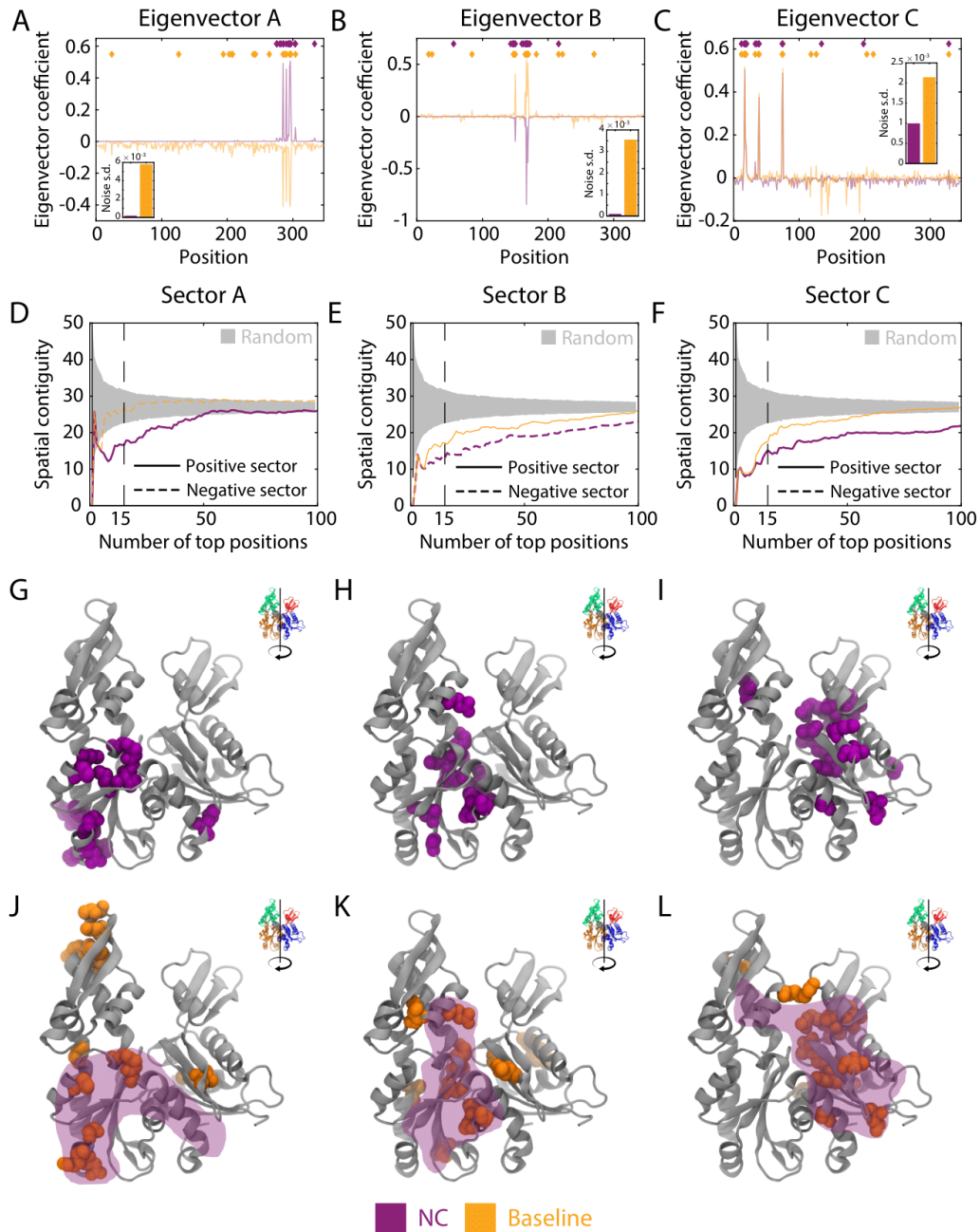
671

672 **Figure 2: NC improves predictions of structural contacts across proteins and**

673 **coevolution methods, and resolves information loss due to subsampling of the set of**

674 **sequences.**

- 675 A) NC increased the number of true-positive structural contacts among the first 50
676 predictions for 10 highly conserved proteins predicted by DCA using DI or
677 Frobenius norm, without or with APC.
- 678 B) MSAs were subsampled across breadth (random sampling) and depth (sorted
679 sampling) of the MSA. Typically, the distribution of Jukes-Cantor distances in the
680 MSA (red) remained essentially unchanged for breadth sampling (green and blue),
681 while it shifted to lower values (as expected) for depth sampling (gold and purple);
682 shown is the KH domain.
- 683 C) NC generally increased the number of true-positive structural contacts among the
684 first 50 predictions relative to DCA employing DI (without APC) across proteins
685 and both breadth and depth sampling (for DI with APC, see Fig. S3). Small
686 decreases occurred for depth sampling of RNase H, thioredoxin, and Kunitz.



687

688 **Figure 3: NC eigenvectors for the actin homolog MreB have lower noise and are more**

689 **spatially contiguous than baseline eigenvectors.**

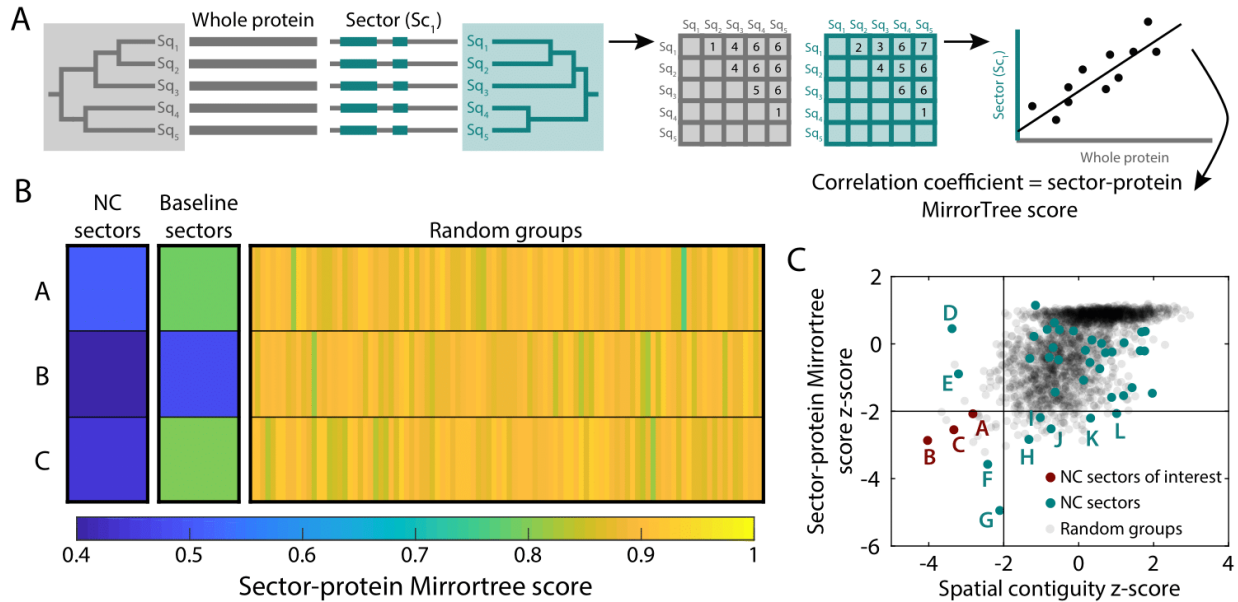
690 A-C) Three eigenvectors with large eigenvalues were identified and paired between

691 baseline coevolution (NMI with APC) and the NC correction for an MSA

692 containing 9,998 sequences of MreB. Aside from the residues with large
693 coefficients, the NC eigenvectors exhibited lower background noise than the
694 baseline eigenvectors. Insets: standard deviations of the eigenvector coefficients
695 after excluding the highest and lowest 50 values.

696 D-F) NC sectors are more spatially contiguous than the corresponding baseline
697 sectors. Sectors were defined based on a sliding cutoff of the most positive or most
698 negative coefficients of each eigenvector in (A-C). Spatial contiguity was defined
699 as the mean pairwise distance between each residue within a sector.

700 G-L) For the 15-residue versions of the NC and baseline sectors (vertical lines in (D-
701 F)), the NC sectors (G-I) are more compact on the three-dimensional structure than
702 the corresponding baseline sectors (J-L). The shaded purple regions in (J-L)
703 represent the NC sector.



704

705 **Figure 4: Sectors are phylogenetically distinct from the entire protein.**

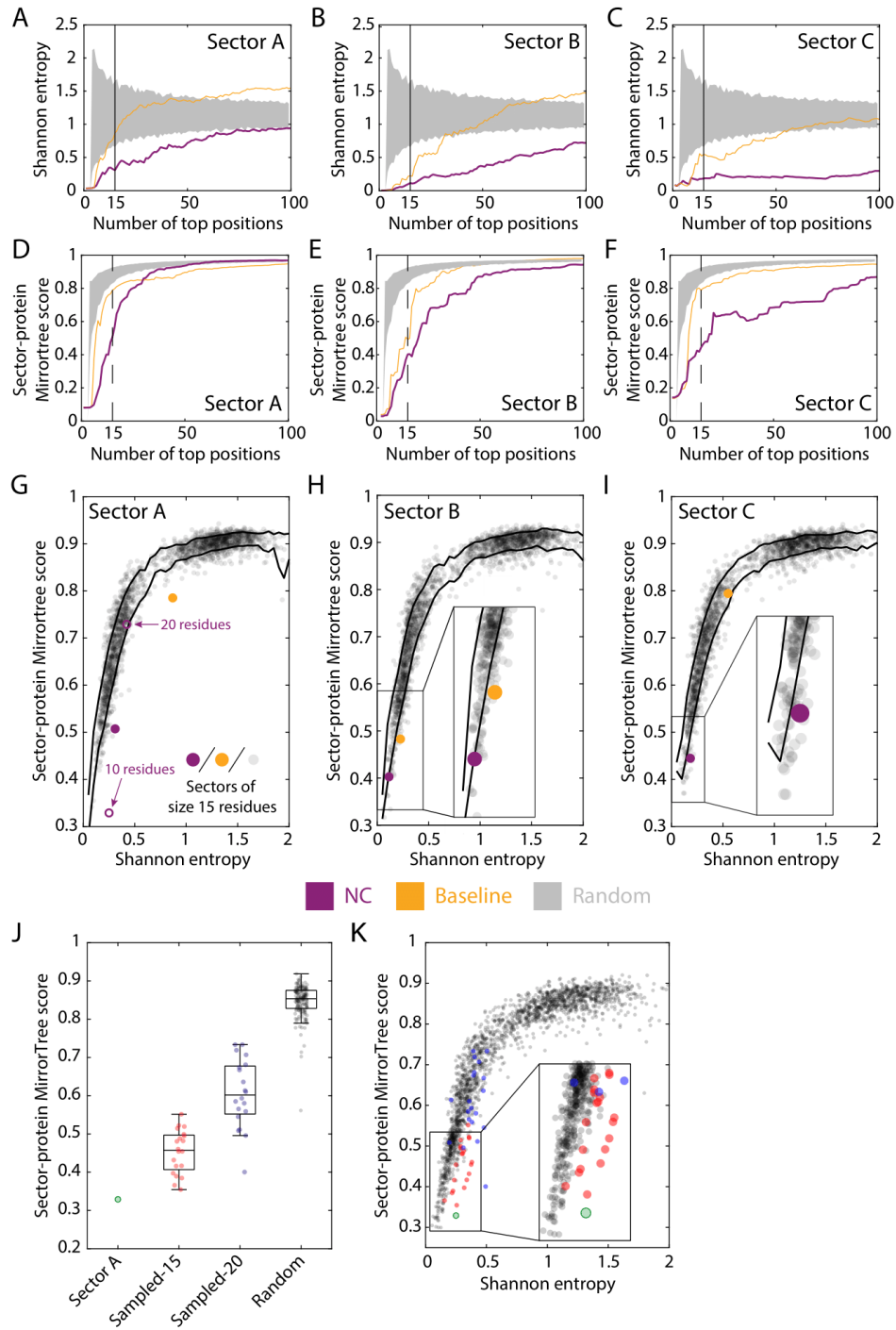
706 A) Repurposing the MirrorTree algorithm (37) to measure the phylogenetic similarity
707 between sectors and the entire protein. The MirrorTree score is defined as the
708 Pearson correlation coefficient between the entries in the two pairwise distance
709 matrices of all sequences within an MSA for the protein versus only the residues
710 in the sector.

711 B) MreB NC sectors A-C (Fig. 3) had lower sector-protein MirrorTree scores than the
712 corresponding baseline sectors, while random groups of 15 residues had
713 MirrorTree scores close to 1 (as expected).

714 C) MreB NC sectors were computed from the 15 most positive or negative coefficients
715 of the 20 eigenvectors with the highest eigenvalues. Among these 40 sectors, the z-

716 scores of the MirrorTree score and the spatial contiguity were <-2 for sectors A-C.

717 Sectors D-L substantially overlapped sectors A-C, and are considered in Fig. 6.



718

719 **Figure 5: Sector-protein MirrorTree scores of residue groups are correlated with**
720 **entropy, but NC sectors have lower MirrorTree scores than expected from entropy**
721 **alone.**

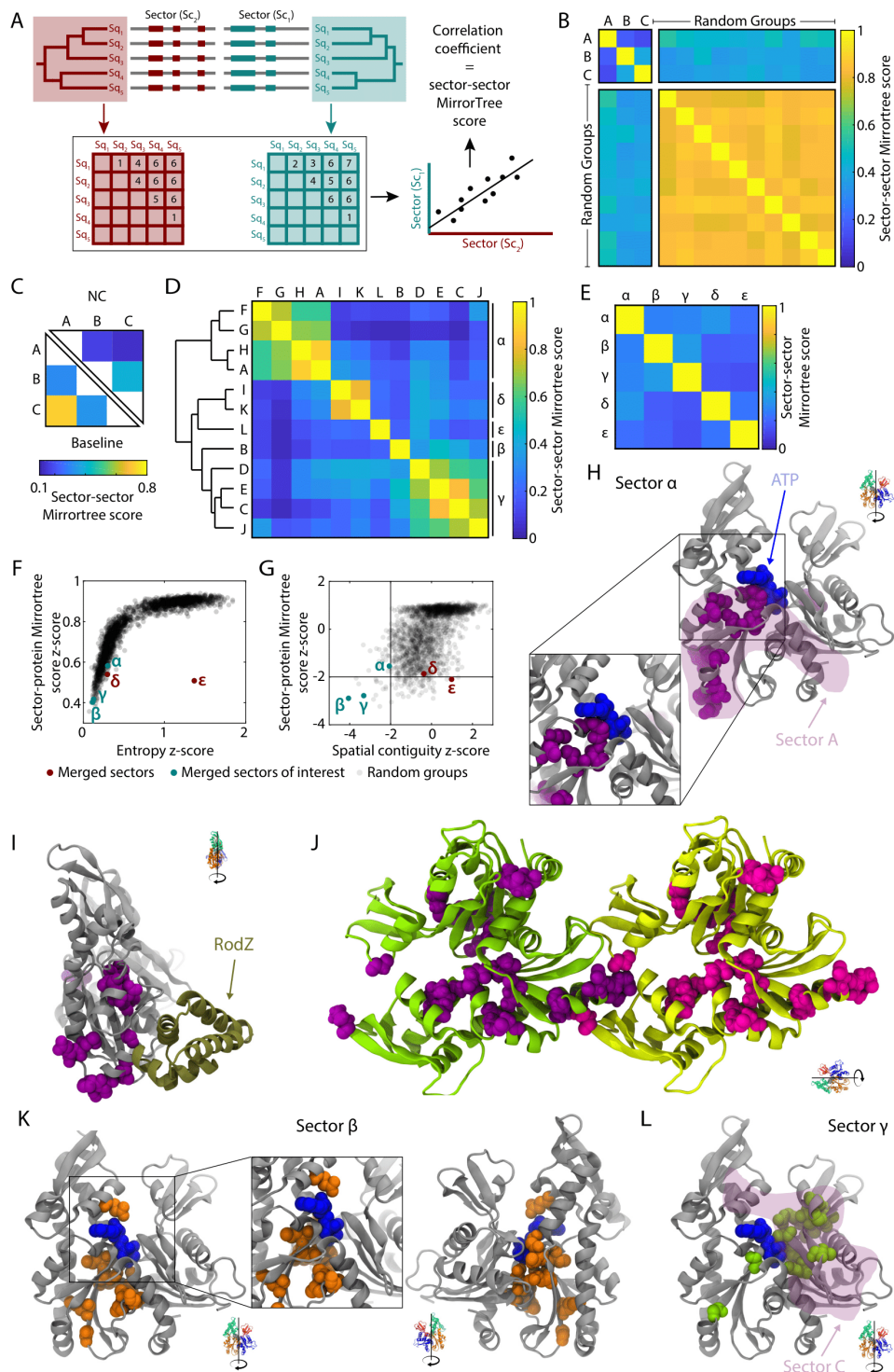
722 A-C) The Shannon entropy of MreB NC sectors A-C (Fig. 3) across size cutoffs is lower
723 than that of the corresponding baseline sectors, indicating that NC selects more
724 conserved residues (albeit entropy is still higher than the cutoff of <0.1 for typically
725 being considered highly conserved). Gray regions represent the entropy of a
726 randomly selected group of residues of the same size.

727 D-F) MirrorTree scores are lower for the NC sectors than for the corresponding
728 baseline sectors. Gray regions represent the MirrorTree scores of a randomly
729 selected group of residues of the same size.

730 G-I) The MirrorTree scores of sectors A-C (filled gold and purple circles) and of
731 random groups of 15 residues (gray). Although MirrorTree score is linked to
732 entropy, NC sectors A and C have MirrorTree scores significantly lower than
733 expected based on entropy alone. In (G), the open purple circles denote the
734 versions of sector A with 10 and 20 residues. Black curves indicate ± 1 standard
735 deviation from the mean MirrorTree score for a given entropy.

736 J) The 10-residue version of NC sector A has lower MirrorTree score than sets of 10
737 residues selected from the 15- and 20-residue versions of the same sector, which
738 are lower than those of random groups of 10 residues. The central mark indicates
739 the median, and the bottom and top edges of the box indicate the 25th and 75th
740 percentiles, respectively. The whiskers extend to the most extreme data points not
741 considered outliers.

742 K) The 10-residue version of NC sector A has a lower MirrorTree score than 10-residue
743 subsets of the 15- and 20-residue versions of the same sector with similar entropy.
744 Same data as in (J). Thus, the 10-residue sector represents a “core” of the most
745 highly coevolving residues.

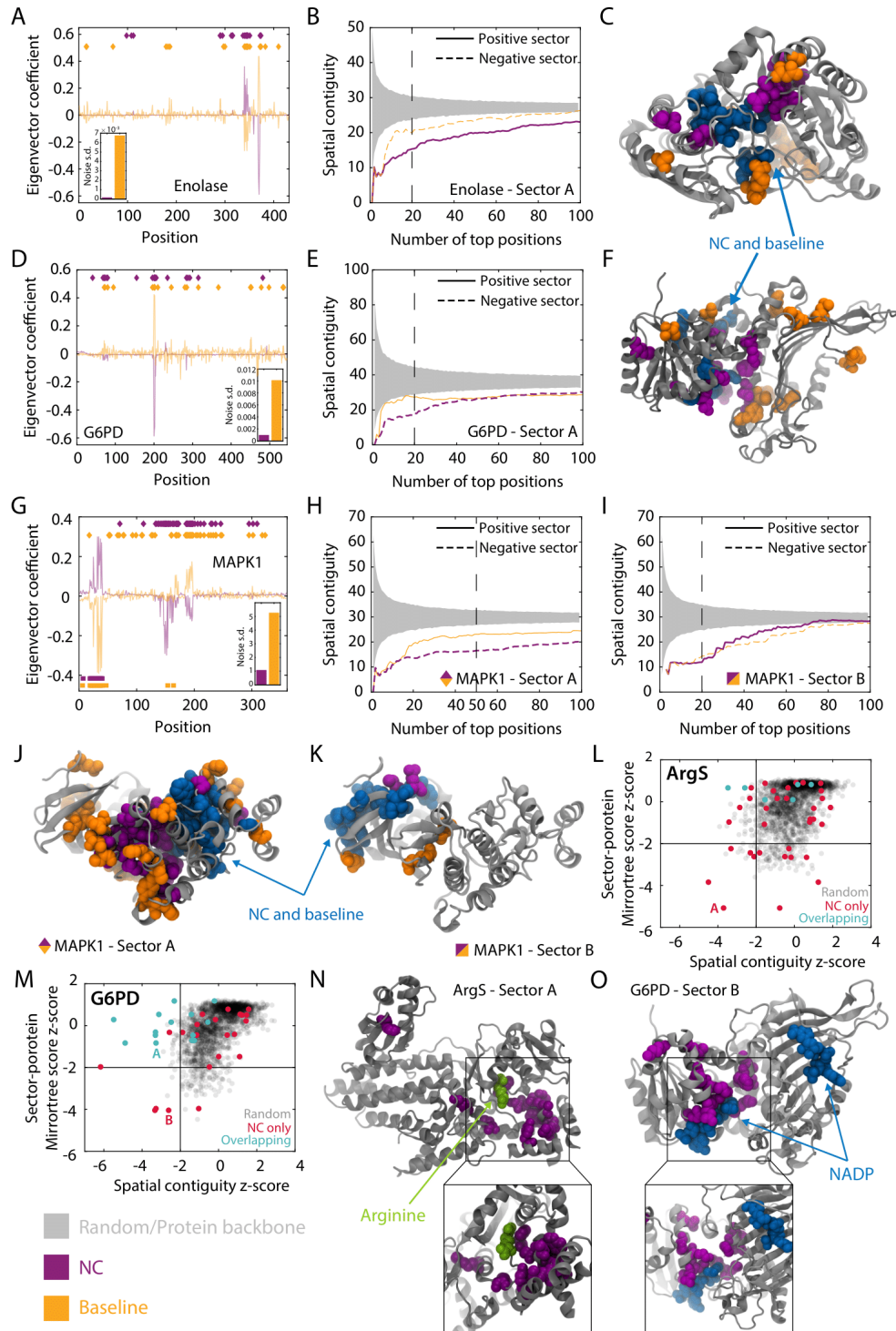


746

747 **Figure 6: MreB NC sectors are generally phylogenetically distinct, and those with**
 748 **phylogenetic overlap collectively overlap with functionally important regions.**

- 749 A) Repurposing the MirrorTree algorithm to measure the phylogenetic similarity
750 between sectors.
- 751 B) MreB NC sectors A, B, and C exhibited low sector-sector MirrorTree scores with
752 each other, but high values with random groups of 15 residues (which also
753 exhibited high MirrorTree scores with each other).
- 754 C) NC sectors A-C have lower sector-sector MirrorTree scores with each other than
755 baseline sectors A-C with each other, indicating that they are more
756 phylogenetically distinct.
- 757 D) Hierarchical clustering of MreB NC sectors A-L (Fig. 4C) based on sector-sector
758 MirrorTree profiles suggests five distinct mega-sectors.
- 759 E-G) The MreB mega-sectors defined by the sum of the clustered eigenvectors
760 exhibited low sector-sector MirrorTree scores with each other (E) as well as low
761 sector-protein MirrorTree scores (F). Mega-sectors α , β , and γ (similar to sectors A-
762 C) exhibited high spatial contiguity (z -score < -2).
- 763 H,I) Mega-sector α was more spatially contiguous than sector A (shaded purple
764 region) (H), and contained residues around the interface with MreB's binding
765 partner RodZ (I).
- 766 J) The 25-residue version of mega-sector α connects the pointed and barbed ends of
767 each subunit in a protofilament.
- 768 K) Mega-sector β (identical to sector B) surrounds the ATP binding pocket.

769 L) Mega-sector γ is more spatially contiguous than sector C (shaded purple region).



770

771 **Figure 7: NC eigenvectors generally improve sector prediction across proteins, and**

772 **enable identification of sectors that are not detectable using the baseline method.**

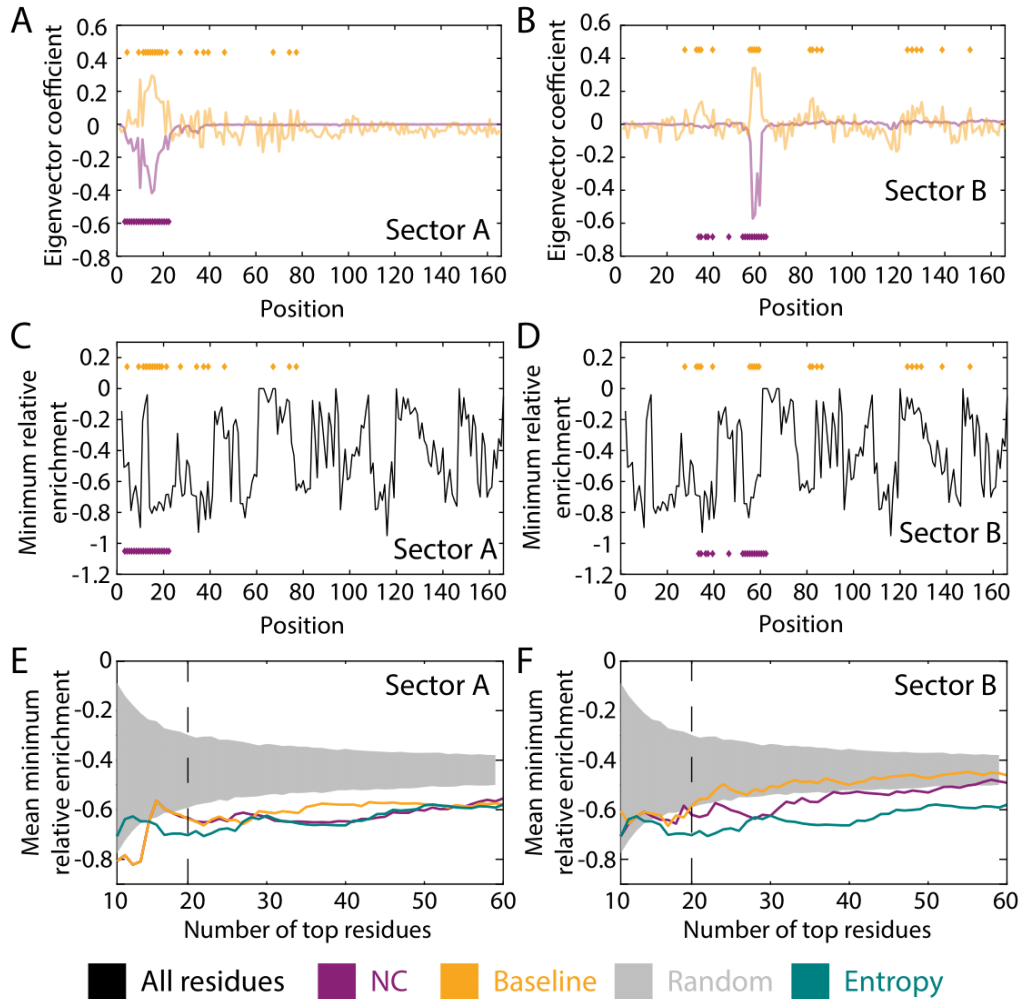
773 A,D,G) NC eigenvectors for enolase (A), G6PD (D), and MAPK1 (G) exhibit lower
774 background noise than the corresponding baseline (NMI with APC)
775 eigenvectors.

776 B,E,H,I) The appropriate NC sectors (positive or negative values of the eigenvector)
777 associated with the eigenvectors in (A,D,G) are more spatially contiguous across
778 size cutoffs than the baseline sectors. Note that the MAPK1 eigenvector was split
779 into a positive sector (H) and a negative sector (I).

780 C,F) The 15-residue versions of the sectors in (B,E) on the crystal structures of enolase
781 (C) and G6PD (F) illustrate the more compact nature of the NC sectors as
782 compared with the baseline sectors.

783 J,K) The 50- and 20-residue versions of the NC sectors in (H,I) are more spatially
784 compact on the structure than the corresponding baseline sectors, and occupy
785 distinct parts of the protein.

786 L-O) For ArgS (L) and G6PD (M), certain high-eigenvalue NC sectors had no
787 obvious baseline counterpart. These NC sectors had low MirrorTree and spatial
788 contiguity z-scores (L,M), and 15-residue versions occupied spatially compact
789 regions around ligands (arginine in (N), NADP in (O)) on the structure (N,O).
790 Thus, NC enables the detection of sectors that are otherwise hidden.



791

792 **Figure 8: NC sectors predict deactivating mutations in H-Ras.**

793 A,B) NC predicts two eigenvectors with much lower background noise than the
794 baseline counterparts. The purple and gold diamonds represent the locations of
795 residues in sectors of size 20.

796 C,D) Fitness data from a screen of binding efficacy of H-Ras to Raf-RBD (57). Shown
797 is the minimum enrichment over all mutations at each position (thus
798 representing maximum deactivation). The purple and gold diamonds represent
799 the locations of residues in sectors of size 20.

800 E,F) Across most sector size cutoffs, the mean minimum relative enrichment was
801 significantly lower than random (gray) for NC sectors A and B and comparable
802 that of the residues with the lowest entropy (teal). NC sectors also outperformed
803 their baseline counterparts.

850 **References**

851

852 1. M. Hollstein, B. Sidransky, B. Vogelstein, C. C. Harris, P53 Mutations in Human
853 Cancers. *Science* **253**, 49-53 (1991).

854 2. M. J. Zvelebil, G. J. Barton, W. R. Taylor, M. J. E. Sternberg, Prediction of protein
855 secondary structure and active sites using the alignment of homologous
856 sequences. *Journal of Molecular Biology* **195**, 957-961 (1987).

857 3. R. S. Dwyer, D. P. Ricci, L. J. Colwell, T. J. Silhavy, N. S. Wingreen, Predicting
858 functionally informative mutations in Escherichia coli BamA using evolutionary
859 covariance analysis. *Genetics* **195**, 443-455 (2013).

860 4. D. S. Marks, L. J. Colwell, R. Sheridan, T. A. Hopf, A. Pagnani, R. Zecchina, C.
861 Sander, Protein 3D structure computed from evolutionary sequence variation.
862 *PLoS ONE* **6** (2011).

863 5. F. Morcos, B. Jana, T. Hwa, J. N. Onuchic, Coevolutionary signals across protein
864 lineages help capture multiple protein conformations. *Proceedings of the National*
865 *Academy of Sciences of the United States of America* **110**, 20533-20538 (2013).

866 6. K. a. Reynolds, R. N. McLaughlin, R. Ranganathan, Hot spots for allosteric
867 regulation on protein surfaces. *Cell* **147**, 1564-1575 (2011).

- 868 7. M. Weigt, R. A. White, H. Szurmant, J. A. Hoch, T. Hwa, Identification of direct
869 residue contacts in protein-protein interaction by message passing. *Proc Natl*
870 *Acad Sci U S A* **106**, 67-72 (2009).
- 871 8. A. F. Bitbol, Inferring interaction partners from protein sequences using mutual
872 information. *PLoS Comput Biol* **14**, e1006401 (2018).
- 873 9. A. F. Bitbol, R. S. Dwyer, L. J. Colwell, N. S. Wingreen, Inferring interaction
874 partners from protein sequences. *Proc Natl Acad Sci U S A* **113**, 12180-12185
875 (2016).
- 876 10. L. Burger, E. van Nimwegen, Accurate prediction of protein-protein interactions
877 from sequence alignments using a Bayesian method. *Mol Syst Biol* **4**, 165 (2008).
- 878 11. T. Gueudre, C. Baldassi, M. Zamparo, M. Weigt, A. Pagnani, Simultaneous
879 identification of specifically interacting paralogs and interprotein contacts by
880 direct coupling analysis. *Proc Natl Acad Sci U S A* **113**, 12186-12191 (2016).
- 881 12. S. Ovchinnikov, H. Kamisetty, D. Baker, Robust and accurate prediction of
882 residue-residue interactions across protein interfaces using evolutionary
883 information. *eLife* (2014).
- 884 13. O. Rivoire, Parsimonious evolutionary scenario for the origin of allostery and
885 coevolution patterns in proteins. *Phys Rev E* **100**, 032411 (2019).

- 886 14. T. A. Hopf, J. B. Ingraham, F. J. Poelwijk, C. P. Scharfe, M. Springer, C. Sander, D.
887 S. Marks, Mutation effects predicted from sequence co-variation. *Nat Biotechnol*
888 **35**, 128-135 (2017).
- 889 15. D. Altschuh, T. Vernet, D. Moras, K. Nagai, Coordinated amino acid changes in
890 homologous protein families. *Protein Engineering* **2**, 193-199 (1988).
- 891 16. W. Atchley, K. Wollenberg, W. Fitch, W. Terhalle, A. Dress, Correlations among
892 amino acid sites in bHLH protein domains: an information theoretic analysis.
893 164-178 (2000).
- 894 17. U. Göbel, C. Sander, R. Schneider, a. Valencia, Correlated mutations and residue
895 contacts in proteins. *Proteins* **18**, 309-317 (1994).
- 896 18. N. Halabi, O. Rivoire, S. Leibler, R. Ranganathan, Protein sectors: evolutionary
897 units of three-dimensional structure. *Cell* **138**, 774-786 (2009).
- 898 19. J. M. Skerker, B. S. Perchuk, A. Siryaporn, E. a. Lubin, O. Ashenberg, M. Goulian,
899 M. T. Laub, Rewiring the Specificity of Two-Component Signal Transduction
900 Systems. *Cell* **133**, 1043-1054 (2008).
- 901 20. S. D. Dunn, L. M. Wahl, G. B. Gloor, Mutual information without the influence of
902 phylogeny or entropy dramatically improves residue contact prediction.
903 *Bioinformatics (Oxford, England)* **24**, 333-340 (2008).

- 904 21. M. Socolich, S. W. Lockless, W. P. Russ, H. Lee, K. H. Gardner, R. Ranganathan,
905 Evolutionary information for specifying a protein fold. *Nature* **437**, 512-518
906 (2005).
- 907 22. F. Morcos, A. Pagnani, B. Lunt, A. Bertolino, D. S. Marks, C. Sander, R. Zecchina,
908 J. N. Onuchic, T. Hwa, M. Weigt, Direct-coupling analysis of residue coevolution
909 captures native contacts across many protein families. *Proc Natl Acad Sci U S A*
910 **108**, E1293-1301 (2011).
- 911 23. L. C. Martin, G. B. Gloor, S. D. Dunn, L. M. Wahl, Using information theory to
912 search for co-evolving residues in proteins. *Bioinformatics* **21**, 4116-4124 (2005).
- 913 24. K. R. Wollenberg, W. R. Atchley, Separation of phylogenetic and functional
914 associations in biological sequences by using the parametric bootstrap. *Proc Natl*
915 *Acad Sci U S A* **97**, 3288-3291 (2000).
- 916 25. M. F. Garcia-Mayoral, D. Hollingworth, L. Masino, I. Diaz-Moreno, G. Kelly, R.
917 Gherzi, C. F. Chou, C. Y. Chen, A. Ramos, The structure of the C-terminal KH
918 domains of KSRP reveals a noncanonical motif important for mRNA
919 degradation. *Structure* **15**, 485-498 (2007).
- 920 26. G. H. Golub, C. F. Van Loan, *Matrix computations*, Johns Hopkins studies in the
921 mathematical sciences (Johns Hopkins University Press, Baltimore, ed. 3rd, 1996),
922 pp. xxvii, 694 p.

- 923 27. M. Ekeberg, C. Lovkvist, Y. Lan, M. Weigt, E. Aurell, Improved contact
924 prediction in proteins: using pseudolikelihoods to infer Potts models. *Phys Rev E*
925 *Stat Nonlin Soft Matter Phys* **87**, 012707 (2013).
- 926 28. S. W. Wang, A. F. Bitbol, N. S. Wingreen, Revealing evolutionary constraints on
927 proteins through sequence analysis. *PLoS Comput Biol* **15**, e1007010 (2019).
- 928 29. R. N. McLaughlin, Jr., F. J. Poelwijk, A. Raman, W. S. Gosal, R. Ranganathan, The
929 spatial architecture of protein function and adaptation. *Nature* **491**, 138-142
930 (2012).
- 931 30. M. Novinec, M. Korenc, A. Caflisch, R. Ranganathan, B. Lenarcic, A. Baici, A
932 novel allosteric mechanism in the cysteine peptidase cathepsin K discovered by
933 computational methods. *Nat Commun* **5**, 3287 (2014).
- 934 31. O. Rivoire, K. A. Reynolds, R. Ranganathan, Evolution-Based Functional
935 Decomposition of Proteins. *PLoS Comput Biol* **12**, e1004817 (2016).
- 936 32. R. G. Smock, O. Rivoire, W. P. Russ, J. F. Swain, S. Leibler, R. Ranganathan, L. M.
937 Gierasch, An interdomain sector mediating allostery in Hsp70 molecular
938 chaperones. *Mol Syst Biol* **6**, 414 (2010).
- 939 33. H. Shi, B. P. Bratton, Z. Gitai, K. C. Huang, How to Build a Bacterial Cell: MreB
940 as the Foreman of E. coli Construction. *Cell* **172**, 1294-1305 (2018).

- 941 34. T. Izore, R. Duman, D. Kureisaite-Ciziene, J. Lowe, Crenactin from *Pyrobaculum*
942 *calidifontis* is closely related to actin in structure and forms steep helical
943 filaments. *FEBS Lett* **588**, 776-782 (2014).
- 944 35. F. van den Ent, L. A. Amos, J. Lowe, Prokaryotic origin of the actin cytoskeleton.
945 *Nature* **413**, 39-44 (2001).
- 946 36. F. van den Ent, L. Amos, J. Lowe, Bacterial ancestry of actin and tubulin. *Curr*
947 *Opin Microbiol* **4**, 634-638 (2001).
- 948 37. R. A. Craig, L. Liao, Phylogenetic tree information aids supervised learning for
949 predicting protein-protein interaction based on distance matrices. *BMC*
950 *Bioinformatics* **8**, 6 (2007).
- 951 38. F. Pazos, A. Valencia, Similarity of phylogenetic trees as indicator of protein-
952 protein interaction. *Protein Eng* **14**, 609-614 (2001).
- 953 39. C. L. Araya, C. Cenik, J. A. Reuter, G. Kiss, V. S. Pande, M. P. Snyder, W. J.
954 Greenleaf, Identification of significantly mutated regions across cancer types
955 highlights a rich landscape of functional molecular alterations. *Nat Genet* **48**, 117-
956 125 (2016).
- 957 40. Z. Hu, B. Ma, H. Wolfson, R. Nussinov, Conservation of polar residues as hot
958 spots at protein interfaces. *Proteins* **39**, 331-342 (2000).
- 959 41. O. B. Ptitsyn, Protein folding and protein evolution: common folding nucleus in
960 different subfamilies of c-type cytochromes? *J Mol Biol* **278**, 655-666 (1998).

- 961 42. T. Teşileanu, L. J. Colwell, S. Leibler, Protein Sectors: Statistical Coupling
962 Analysis versus Conservation. *PLOS Computational Biology* **11**, e1004091 (2015).
- 963 43. I. Anishchenko, S. Ovchinnikov, H. Kamisetty, D. Baker, Origins of coevolution
964 between residues distant in protein 3D structures. *Proc Natl Acad Sci U S A* **114**,
965 9122-9127 (2017).
- 966 44. B. P. Bratton, J. W. Shaevitz, Z. Gitai, R. M. Morgenstein, MreB polymers and
967 curvature localization are enhanced by RodZ and predict E. coli's cylindrical
968 uniformity. *Nat Commun* **9**, 2797 (2018).
- 969 45. A. Colavin, H. Shi, K. C. Huang, RodZ modulates geometric localization of the
970 bacterial actin MreB to regulate cell shape. *Nat Commun* **9**, 1280 (2018).
- 971 46. T. G. Spring, F. Wold, The purification and characterization of Escherichia coli
972 enolase. *J Biol Chem* **246**, 6797-6802 (1971).
- 973 47. D. N. Wright, W. R. Lockhart, Effects of Growth Rate and Limiting Substrate on
974 Glucose Metabolism in Escherichia Coli. *J Bacteriol* **89**, 1082-1085 (1965).
- 975 48. S. L. Pelech, J. S. Sanghera, M. Daya-Makin, Protein kinase cascades in meiotic
976 and mitotic cell cycle control. *Biochem Cell Biol* **68**, 1297-1330 (1990).
- 977 49. T. W. Sturgill, J. Wu, Recent progress in characterization of protein kinase
978 cascades for phosphorylation of ribosomal protein S6. *Biochim Biophys Acta* **1092**,
979 350-357 (1991).

- 980 50. I. N. Hirshfield, H. P. Bloemers, The biochemical characterization of two mutant
981 arginyl transfer ribonucleic acid synthetases from Escherichia coli K-12. *J Biol*
982 *Chem* **244**, 2911-2916 (1969).
- 983 51. S. L. Dove, J. K. Joung, A. Hochschild, Activation of prokaryotic transcription
984 through arbitrary protein-protein contacts. *Nature* **386**, 627-630 (1997).
- 985 52. J. K. Joung, E. I. Ramm, C. O. Pabo, A bacterial two-hybrid selection system for
986 studying protein-DNA and protein-protein interactions. *Proc Natl Acad Sci U S A*
987 **97**, 7382-7387 (2000).
- 988 53. W. A. Lim, R. T. Sauer, Alternative packing arrangements in the hydrophobic
989 core of lambda repressor. *Nature* **339**, 31-36 (1989).
- 990 54. C. W. Johnson, D. Reid, J. A. Parker, S. Salter, R. Knihtila, P. Kuzmic, C. Mattos,
991 The small GTPases K-Ras, N-Ras, and H-Ras have distinct biochemical properties
992 determined by allosteric effects. *J Biol Chem* **292**, 12981-12993 (2017).
- 993 55. C. Wellbrock, M. Karasarides, R. Marais, The RAF proteins take centre stage. *Nat*
994 *Rev Mol Cell Biol* **5**, 875-885 (2004).
- 995 56. I. A. Prior, P. D. Lewis, C. Mattos, A comprehensive survey of Ras mutations in
996 cancer. *Cancer Res* **72**, 2457-2467 (2012).
- 997 57. P. Bandaru, N. H. Shah, M. Bhattacharyya, J. P. Barton, Y. Kondo, J. C. Cofsky, C.
998 L. Gee, A. K. Chakraborty, T. Kortemme, R. Ranganathan, J. Kuriyan,

- 999 Deconstruction of the Ras switching cycle through saturation mutagenesis. *Elife* 6
1000 (2017).
- 1001 58. R. Do *et al.*, Exome sequencing identifies rare LDLR and APOA5 alleles
1002 conferring risk for myocardial infarction. *Nature* **518**, 102-106 (2015).
- 1003 59. H. Q. Nguyen, J. Roy, B. Harink, N. P. Damle, N. R. Latorraca, B. C. Baxter, K.
1004 Brower, S. A. Longwell, T. Kortemme, K. S. Thorn, M. S. Cyert, P. M. Fordyce,
1005 Quantitative mapping of protein-peptide affinity landscapes using spectrally
1006 encoded beads. *Elife* **8** (2019).
- 1007 60. A. W. Senior, R. Evans, J. Jumper, J. Kirkpatrick, L. Sifre, T. Green, C. Qin, A.
1008 Zidek, A. W. R. Nelson, A. Bridgland, H. Penedones, S. Petersen, K. Simonyan, S.
1009 Crossan, P. Kohli, D. T. Jones, D. Silver, K. Kavukcuoglu, D. Hassabis, Improved
1010 protein structure prediction using potentials from deep learning. *Nature* **577**, 706-
1011 710 (2020).
- 1012 61. T. Madden, The BLAST Sequence Analysis Tool. 2002 Oct 9 [Updated 2003 Aug
1013 13]. *The NCBI Handbook [Internet]. Bethesda (MD): National Center for Biotechnology*
1014 *Information (US)* (2002).
- 1015 62. T. Tatusova, S. Ciufu, B. Fedorov, K. O'Neill, I. Tolstoy, RefSeq microbial
1016 genomes database: new representation and annotation strategy. *Nucleic Acids Res*
1017 **42**, D553-559 (2014).

- 1018 63. F. Sievers, A. Wilm, D. Dineen, T. J. Gibson, K. Karplus, W. Li, R. Lopez, H.
1019 McWilliam, M. Remmert, J. Soding, J. D. Thompson, D. G. Higgins, Fast, scalable
1020 generation of high-quality protein multiple sequence alignments using Clustal
1021 Omega. *Mol Syst Biol* 7, 539 (2011).
1022